

This is the accepted manuscript made available via CHORUS. The article has been published as:

Anharmonic effects in atomic hydrogen: Superconductivity and lattice dynamical stability

Miguel Borinaga, Ion Errea, Matteo Calandra, Francesco Mauri, and Aitor Bergara

Phys. Rev. B **93**, 174308 — Published 17 May 2016

DOI: [10.1103/PhysRevB.93.174308](https://doi.org/10.1103/PhysRevB.93.174308)

Anharmonic effects in atomic hydrogen: superconductivity and lattice dynamical stability

Miguel Borinaga,^{1,2} Ion Errea,^{2,3} Matteo Calandra,⁴ Francesco Mauri,^{4,5} and Aitor Bergara^{1,2,6}

¹*Centro de Física de Materiales CFM, CSIC-UPV/EHU,
Paseo Manuel de Lardizabal 5, 20018 Donostia/San Sebastián, Basque Country, Spain*

²*Donostia International Physics Center (DIPC), Manuel Lardizabal pasealekua 4,
20018 Donostia/San Sebastián, Basque Country, Spain*

³*Fisika Aplicatua 1 Saila, EUITI Bilbao, University of the Basque Country (UPV/EHU),
Rafael Moreno “Pitxitxi” Pasealekua 3, 48013 Bilbao, Basque Country, Spain*

⁴*IMPMC, UMR CNRS 7590, Sorbonne Universités - UPMC Univ. Paris 06,
MNHN, IRD, 4 Place Jussieu, F-75005 Paris, France*

⁵*Dipartimento di Fisica, Università di Roma La Sapienza, Piazzale Aldo Moro 5, I-00185 Roma, Italy*

⁶*Departamento de Física de la Materia Condensada,
University of the Basque Country (UPV/EHU), 48080 Bilbao, Basque Country, Spain*

(Dated: April 19, 2016)

We present first-principles calculations of metallic atomic hydrogen in the 400-600 GPa pressure range in a tetragonal structure with space group $I4_1/amd$, which is predicted to be its first atomic phase. Our calculations show a band structure close to the free-electron-like limit due to the high electronic kinetic energy induced by pressure. Bands are properly described even in the independent electron approximation fully neglecting the electron-electron interaction. Linear-response harmonic calculations show a dynamically stable phonon spectrum with marked Kohn anomalies. Even if the electron-electron interaction has a minor role in the electronic bands, the inclusion of electronic exchange and correlation in the density response is essential to obtain a dynamically stable structure. Anharmonic effects, which are calculated within the stochastic self-consistent harmonic approximation, harden high-energy optical modes and soften transverse acoustic modes up to a 20% in energy. Despite a large impact of anharmonicity has been predicted in several high-pressure hydrides, here the superconducting critical temperature is barely affected by anharmonicity, as it is lowered from its harmonic 318 K value only to 300 K at 500 GPa. We attribute the small impact of anharmonicity on superconductivity to the absence of softened optical modes and the fairly uniform distribution of the electron-phonon coupling among the vibrational modes.

I. INTRODUCTION

The recent measurement of a superconducting critical temperature (T_c) of 203 K in the sulfur hydrogen system¹, a temperature reachable on Earth’s surface, is a major breakthrough in the field of superconductivity. It ultimately validates Ashcroft’s idea that hydrogen and hydrogen-dominant metallic compounds can be high-temperature superconductors^{2,3}. This measurement offers new hopes to find sooner than later room-temperature superconductivity in other hydrogen-rich compounds or hydrogen itself. Indeed, since the advent of modern *ab initio* calculations for the electron-phonon interaction, many theoretical calculations have predicted astonishingly high T_c values for hydrogen at megabar pressures, both in molecular and atomic phases, the largest T_c values predicted for any compound up to date^{4–10}.

Thus far, five solid phases of hydrogen have been determined, all of them molecular and insulating. However, a sixth metallic one has been recently claimed to be found¹¹. Phase I is thought to be a molecular solid of quantum rotors on a hexagonal close packed lattice¹². It is found in a wide pressure and temperature range up to the melting curve, which has a maximum of \sim 1000 K around 65 GPa^{13,14}. Phase II appears between ap-

proximately 50-150 GPa and only below 150 K, temperature at which it transforms back to phase I¹⁵. Hydrogen adopts phase III above 150 GPa up to at least 360 GPa^{16,17}. Recent experiments have determined that this phase transforms to phase IV at around 200 K in the 240-325 GPa pressure range^{18–20}, which might melt close to room temperature²¹. Transition from phase IV to V occurs at 325 GPa, the last one existing probably up to the dissociation pressure²². Finally, a new work claims to have found phase VI by cooling down phase V below 200-220 K. This new phase could be metallic, but further work is expected to confirm this result¹¹. In any case, and even though the goal seems closer than ever, the quest for metallic hydrogen continues. Extrapolation of optical experiments²³ predicted a metalization pressure of around 450 GPa, which was expected to occur due to the overlap between the valence and conduction bands in the molecular state before molecular dissociation^{24,25}. However, works in Ref. 22 and 11 suggest metalization might occur together with molecular dissociation. In any case, state-of-the-art static diamond anvil cell techniques²⁶ will allow promising future experiments that are expected to shine light on this long standing quest.

Even though it has not been experimentally confirmed yet, recent quantum Monte Carlo calculations including anharmonicity for the zero-point energy²⁷ predict hydro-

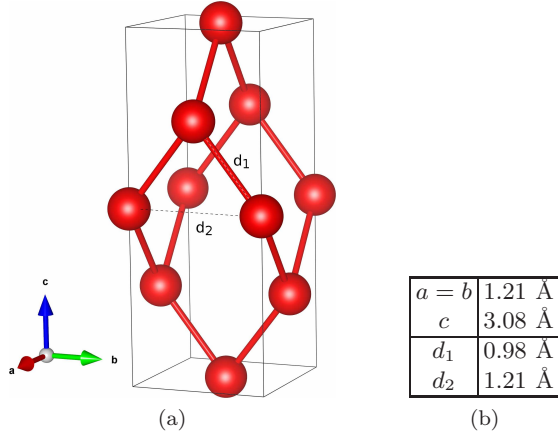


Figure 1. (a) Conventional unit cell of $I4_1/amd$ hydrogen. (b) $a = b$ and c lattice parameters as well as the two different interatomic distances d_1 and d_2 of $I4_1/amd$ hydrogen at 500 GPa.

gen should undergo a transition to a metallic and atomic tetragonal $I4_1/amd$ phase (shown in Fig. 1) around 374 GPa, which had been predicted before²⁸. It seems the inclusion of anharmonicity is important to describe the boundaries of phases I, II, III, and IV²⁹, as well as to estimate the vibron energies in phases III and IV^{30,31}. Nevertheless, even if anharmonicity has a huge impact on the superconducting properties of many hydrides^{32–37}, the potential impact of anharmonicity in the large T_c values predicted for hydrogen^{4–10} remains unexplored. Considering that in aluminum^{36,37}, palladium³⁴, and platinum hydrides³⁵, as well as in the record superconductor H_3S ³² anharmonicity suppresses the electron-phonon coupling as it tends to harden optical H-character phonon modes, one might expect that anharmonicity might strongly impact superconductivity in hydrogen too.

In this work we present an *ab initio* analysis based on density-functional theory (DFT) of electronic and vibrational properties of $I4_1/amd$ hydrogen in the 400–600 GPa pressure range. While in Ref. 8 vibrational and superconducting properties of this possible first structure of atomic hydrogen phase are analyzed holding to the harmonic approach, our goal is to elucidate the impact of anharmonicity in those properties plus its implications in lattice stability. Our results show a close to free-electron-like behavior, as the DFT band structure is perfectly described even if electron-electron interaction is fully neglected. The harmonic phonons calculated within linear-response density-functional perturbation theory (DFPT)³⁸ show the system is dynamically stable even if marked Kohn anomalies are present. Despite the minor role of electron-electron interaction in the electronic states, electronic exchange becomes of vital importance to ensure the dynamical stability of the system. We have included anharmonic effects using the stochastic self-consistent harmonic approximation (SSCHA)^{34,35} and observed the phonon spectrum is significantly modified. However, in contrast to many superconducting

hydrides^{32,34–37}, the superconducting T_c obtained within the harmonic approximation is barely modified by anharmonicity, as it is only suppressed by a 6%.

The paper is organized as follows. In Sec. II we overview the computational details and methods used throughout. In Sec. III we present and analyze the obtained results. Finally, we present a summary of our conclusions in Sec. IV.

II. COMPUTATIONAL DETAILS

We performed our DFT calculations within the Perdew-Burke-Ernzerhof parametrization of the generalized-gradient approximation³⁹. The electron-proton interaction was considered making use of an ultrasoft pseudopotential as implemented in QUANTUM ESPRESSO⁴⁰. Due to the large kinetic energy of the electrons, a proper convergence of the electronic properties and phonon frequencies required a dense $80 \times 80 \times 80$ \mathbf{k} -mesh and 0.05 Ry Hermite-Gaussian electronic smearing for the electronic integrations in the first Brillouin zone (BZ). An energy cutoff of 100 Ry was necessary for expanding the wave-functions in the plane-wave basis.

Phonon frequencies were calculated within DFPT as implemented in QUANTUM ESPRESSO⁴⁰ in a $6 \times 6 \times 6$ \mathbf{q} -point grid in the BZ. Fourier interpolation was used to obtain the phonon spectra along high-symmetry lines. We find convenient to split the calculated dynamical matrices at a given wave-vector as $D(\mathbf{q}) = D_p(\mathbf{q}) + D_e(\mathbf{q})$. D_p represents the contribution of the proton-proton Coulomb interaction to the dynamical matrix, which can be estimated analytically with an Ewald summation. D_e contains the effect of the electronic response to the proton motion in the dynamical matrix. Besides DFPT, we have also estimated D_e making use of the free-electron Lindhard response function within the Random Phase Approximation (RPA) as in Ref. 41. In the latter approach the dynamical matrix is analytical at any \mathbf{q} so that we have not restricted the calculations to the $6 \times 6 \times 6$ grid.

Electron-phonon matrix elements were also calculated within DFPT in a $6 \times 6 \times 6$ \mathbf{q} -point grid. Converging the double Dirac delta in the equation for the phonon linewidth required a $100 \times 100 \times 100$ denser \mathbf{k} -point mesh. The superconducting T_c was calculated solving isotropic Migdal-Eliashberg equations^{42,43}, considering that for large electron-phonon coupling constants McMillan's equation underestimates T_c ⁴⁴.

We use the SSCHA^{34,35} to calculate the anharmonic renormalization of the phonon spectrum. The SSCHA is a variational method in which the vibrational free energy is minimized with respect to a trial harmonic density matrix. This minimization process requires the calculation of forces acting on atoms in supercells for different configurations created with the trial density matrix. These forces were calculated in a $3 \times 3 \times 3$ supercell making use of DFT with the same parameters as the DFPT phonon

calculations. This yielded phonon frequencies in a commensurate $3 \times 3 \times 3$ \mathbf{q} -point grid. The difference between the harmonic and anharmonic dynamical matrices was interpolated to the finer $6 \times 6 \times 6$ grid. The anharmonic correction to the superconducting T_c was calculated combining the SSCHA dynamical matrices with the calculated electron-phonon deformation potential within DFPT as explained in Ref. 34.

III. RESULTS AND DISCUSSION

A. Electronic structure

Hydrogen, containing a single proton and an electron, is supposed to leave its common molecular nature under a sufficient high pressure to form a metal similar to the alkalis. In the high pressure limit the dominant electronic kinetic energy would be responsible for ending up with a free-electron-like metal. However, in the analyzed pressure range we are still close to the dissociation/metalization pressure²³ and the problem is not as simple as one could imagine *a priori*.

Fig. 2a shows the electronic band structure of $I4_1/AMD$ hydrogen at 500 GPa. The bands present a huge dispersion, associated to the dominating kinetic term in the energies of the electronic states. The calculated band structure is not far from the free-electron approximation, the main difference being the band gaps opened at the border of the BZ and whenever band crossing occurs due to the interaction of the electrons with the proton lattice. It is interesting to point out that if we consider the independent electron approximation, just keeping the $V_{e,p}$ term that gives the electron-proton interaction in the V_{scf} self-consistent potential and neglecting the V_H Hartree and V_{xc} electron-electron interactions (see Appendix for details), the resulting bands match almost perfectly with the DFT ones. Therefore, we can conclude that main differences with the free-electron approximation are due to the large proton-electron interaction, and that the interaction between the electrons is not giving any significant contribution to the band structure. Fig. 2b shows the Fermi surface, which is quite spherical. However, the sphere shows some open areas around the high symmetry point N, where it touches the BZ boundary and a band gap is opened.

B. Vibrational properties

In Fig. 3 we show the calculated phonon dispersion in tetragonal $I4_1/AMD$ hydrogen at 500 GPa within DFPT. We also show the phonons at 400 and 600 GPa, but due to the minor qualitative changes we will focus just in the 500 GPa spectrum, as the analysis should be valid for all the pressure range. The system clearly is dynamically stable, but there are some branches with strong Kohn anomalies⁴⁵, specially the low energy transverse

acoustic branch. Indeed, as shown in Fig. 3, \mathbf{q} -points at which the anomalies appear coincide with $|\mathbf{q} + \mathbf{G}| = 2k_f$, where k_f is the Fermi wave-vector and \mathbf{G} the reciprocal lattice vector that brings \mathbf{q} back into the BZ. Considering the validity of the free-electron-like approximation to describe the electronic band structure, we have calculated the phonon dispersion within this approximation, assuming that the D_e contribution to the dynamical matrix can be calculated with the Lindhard response function at the RPA level as in Ref. 41, therefore, neglecting correlation and exchange in the electronic response. In this free-electron limit we can obtain the spectra along high-symmetry lines without any Fourier interpolation, evidencing the presence of the Kohn anomalies at the $|\mathbf{q} + \mathbf{G}| = 2k_f$ points, and confirming that the kinks present in the DFPT result are Kohn anomalies.

Nevertheless, the Lindhard RPA spectrum completely differs from the *ab initio* calculations. The intensity of the Kohn anomalies is much stronger and the transverse acoustic modes become unstable with imaginary frequencies. Therefore, even though the electronic band structure could be understood within the free-electron-like approximation, phonons seem to be far from this picture, contrary to the case of sodium^{41,46}. This fact also questions the stability of the $I4_1/AMD$ tetragonal phase in the ultimate high-pressure limit where the electrons are expected to be free. If we split the dynamical matrix in the D_p and D_e terms, we note that each of them scales differently with the average inter-electronic distance parameter r_s : D_p always scales as r_s^{-3} , while, in the Lindhard RPA, D_e scales as $r_s^{-2}(r_s + C)$, where C is always positive and of the order of unity. Therefore, in the very large pressure limit with small r_s , the D_p contribution is expected to dominate over the electronic contribution. In Fig. 4 we present the dispersion of the root of the eigenvalues of each contribution separately. This represents the phonon spectra that would be obtained from each contribution independently. In our case, phonons associated to D_p are already unstable and the contribution from D_e is not enough to stabilize them. This is the reason why the Lindhard RPA phonons have imaginary frequencies. As in the high-pressure limit D_p will dominate over D_e , the tetragonal $I4_1/AMD$ will not become stable at very large pressure, but more symmetric and compact structures with positive eigenvalues of D_p (as fcc or bcc) will be favored.

In order to better understand the discrepancy between the *ab initio* DFPT and the Lindhard RPA spectra, we have made several calculations based on linear-response theory trying to disentangle the different contributions to the final phonon spectra. The calculation of D_e requires not only the knowledge of the electronic density n but also its linear change δn with respect to ionic displacements³⁸. This last term can be calculated from the interacting electronic density-response function χ , which requires first the knowledge of the non-interacting response χ_0 , and second to solve an integral Dyson-like equation where the linear change of the self-consistent

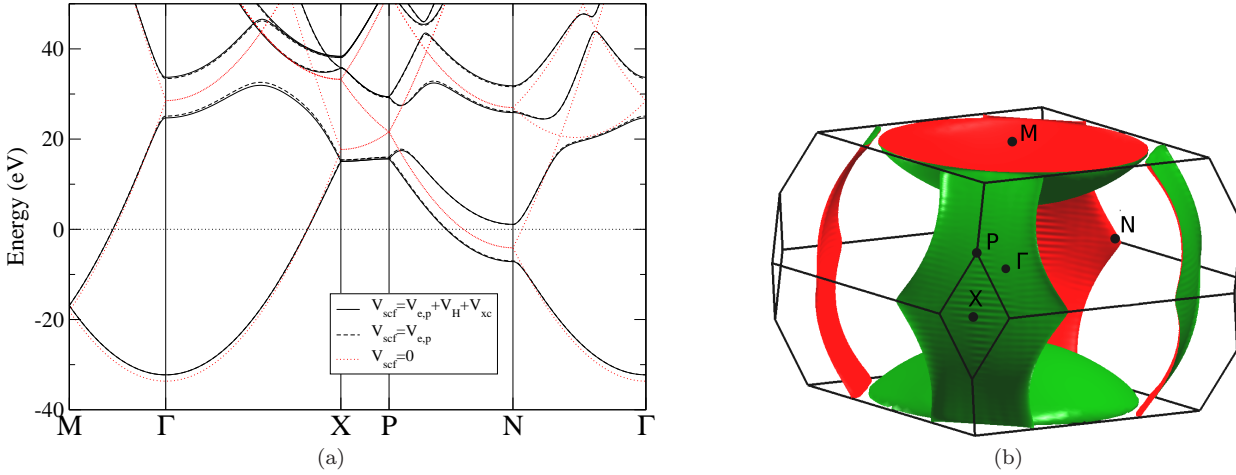


Figure 2. (a) Electronic band structure of $I4_1/amd$ hydrogen at 500 GPa calculated within DFT, where the self-consistent potential is $V_{scf} = V_{e,p} + V_H + V_{xc}$. Bands obtained within the free-electron approach ($V_{scf} = 0$) and the independent-electron approach ($V_{scf} = V_{e,p}$) are also shown. The origin of energy (black dotted line) corresponds to the Fermi level. (b) Fermi surface plot.

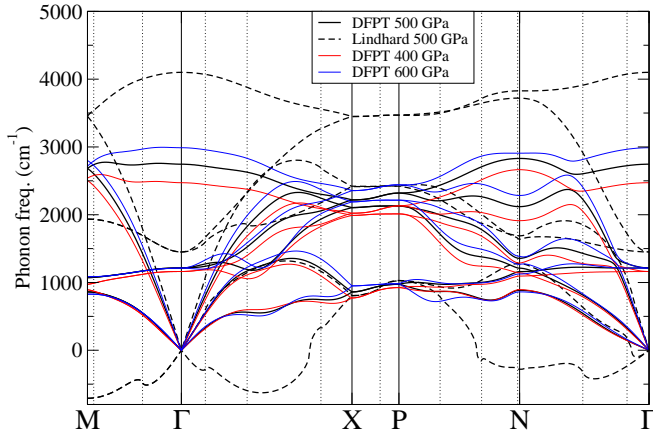


Figure 3. Phonon spectra of $I4_1/amd$ hydrogen calculated within DFPT at several pressures. At 500 GPa phonons calculated within the Lindhard RPA formulation are also shown. Dotted vertical black lines indicate \mathbf{q} -points satisfying $|\mathbf{q} + \mathbf{G}| = 2k_f$, where Kohn anomalies are expected to appear.

potential δV_{scf} takes part (see [Appendix](#)). Although it requires a cumbersome sum over excited state, χ_0 can be calculated directly from the eigenvalues and eigenstates obtained with the unperturbed V_{scf} self-consistent potential. Combining different approximations in V_{scf} to calculate χ_0 and δV_{scf} to calculate χ , the relevant contributions to the dynamical matrices can be unveiled. For instance, in the Lindhard RPA limit χ_0 is built from free-electron bands ($V_{scf} = 0$) and exchange-correlation is neglected to build χ ($\delta V_{scf} = \delta V_{e,p} + \delta V_H$), limit in which D_e is reduced to a simple analytical expression⁴¹. Here, we avoid the explicit calculation of χ_0 and χ by calculating δn making use of DFPT. In this case, the Sternheimer equation is solved self-consistently neglect-

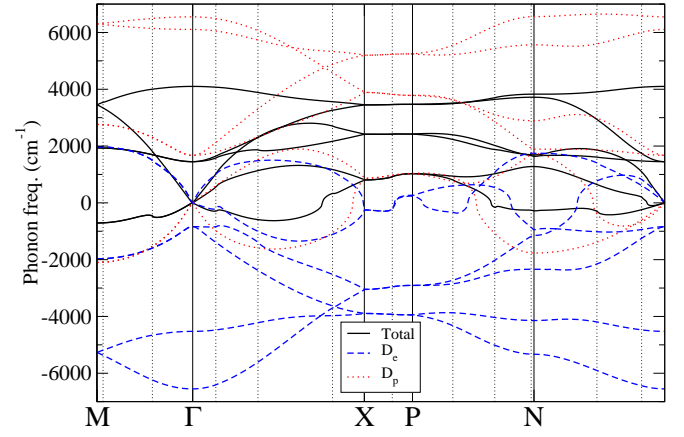


Figure 4. Lindhard RPA phonons of $I4_1/amd$ hydrogen at 500 GPa, decomposed into the contributions coming from the D_p and D_e terms. Dotted vertical lines indicate \mathbf{q} -points satisfying $|\mathbf{q} + \mathbf{G}| = 2k_f$, where Kohn anomalies appear.

ing different terms in V_{scf} and δV_{scf} , which is equivalent to making different approaches to χ_0 and χ respectively. In those cases when a different scheme is adopted for V_{scf} and δV_{scf} translational invariance is not satisfied anymore. We overcome this difficulty imposing the acoustic sum rule (ASR) *a posteriori* (see [Appendix](#) for technical details).

In Fig. 5 we show four phonon spectra with different combination of neglected terms in V_{scf} and δV_{scf} . First, we show the spectrum obtained by neglecting any electron-electron interaction in the unperturbed Hamiltonian ($V_{scf} = V_{e,p}$), but keeping all the terms in its linear perturbation $\delta V_{scf} = \delta V_{e,p} + \delta V_H + \delta V_{xc}$. We obtain exactly the same result as in the previously calculated full DFPT phonons (see Fig. 9 in [Appendix](#) for a

comparison), remarking the insignificant role of electron-electron interaction in the electronic bands and, consequently, in χ_0 . Second, we show the phonons calculated neglecting electron-electron interaction in V_{scf} again, but this time neglecting the exchange and correlation term in δV_{scf} . This is equivalent to calculating χ_0 as in the previous case, but calculating χ within the RPA. Third, we show a consistent Hartree-level calculation where, compared to the previous one, we obtain a quantitatively different but qualitatively identical spectrum in which instabilities remain. Finally, we show the dispersion obtained with free electrons ($V_{scf} = 0$) but using the full linear perturbation going beyond the RPA. Comparing the free-electron RPA calculation in Fig. 3 with the one including exchange-correlation effects for the response in Fig. 5, it can be confirmed that including exchange and correlation in δV_{scf} (and therefore in χ) is determinant for obtaining dynamically stable phonons. However, due to the strong electron-proton interaction, including $V_{e,p}$ in the self-consistent potential is necessary to obtain good quantitative results.

Analyzing these different calculations, we conclude that, despite the electronic kinetic energy dominates and the electron-electron interaction plays a negligible role in the band structure, going beyond the RPA including exchange-correlation effects in the calculation of the electronic response is crucial. Indeed, exchange-correlation effects in the response to the proton motion make tetragonal $I4_1/AMD$ atomic hydrogen dynamically stable. This calamitous failure of the RPA is related to the self-interaction error associated to the Hartree potential, which underestimates the high electronic density around the protons up to a 9% at 500 GPa. We have checked that similar phonons are obtained for different approximations of the exchange-correlation potential^{47,48}. This is not the case in the molecular case at lower pressures, where correlation clearly has an effect in the energies of molecular vibrons⁴⁹.

Even if exchange-correlation effects guarantee the stability of the tetragonal $I4_1/AMD$ atomic structure of hydrogen, this conclusion is drawn exclusively at the harmonic level. In Fig. 6 we compare the harmonic DFPT phonon spectra with the anharmonic spectra obtained within the SSCHA. Anharmonicity is quite strong, as phonon frequencies are affected up to a 20% in the transverse acoustic branch in the Γ -N path. Transverse acoustic branches are in general specially vulnerable as their energies are considerably lowered. Consequently, one could expect anharmonic effects to increase the zero-point displacement of the atoms, bringing atomic hydrogen closer to quantum melting. According to our calculations, however, $I4_1/AMD$ hydrogen is not melted if we hold to the quantum limit of the Lindemann criterion, which states quantum melting occurs when the Root Mean Square (RMS) displacements of atoms are around 27 – 30% of the interatomic distances⁵⁰. While in the harmonic approach we obtain RMS displacements of a 20.3% and a 16.4% relative to the two different inter-

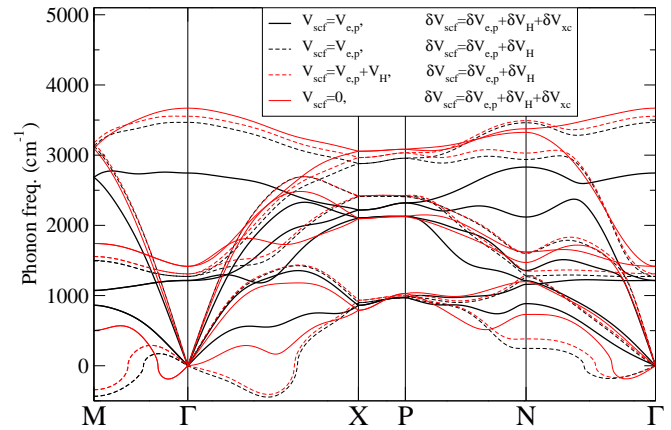


Figure 5. Phonon spectra of $I4_1/AMD$ hydrogen at 500 GPa within different approximations for the unperturbed self-consistent potential V_{scf} and its linear perturbation δV_{scf} . Calculations are performed within the DFPT formalism. The ASR has been imposed *a posteriori* in every case except in the pure Hartree case ($V_{scf} = V_{e,p} + V_H$, $\delta V_{scf} = \delta V_{e,p} + \delta V_H$).

P (GPa)	Mode	ω_h (cm ⁻¹)	ω_{anh} (cm ⁻¹)
400	E_g	1161.8	-
	B_{1g}	2472.2	-
500	E_g	1214.6	1187.9
	B_{1g}	2745.4	2769.8
600	E_g	1212.4	-
	B_{1g}	2988.4	-

Table I. Raman active modes of $I4_1/AMD$ hydrogen in the 400–600 GPa pressure range. Harmonic and anharmonic frequencies are represented as ω_h and ω_{anh} respectively.

atomic distances d_1 and d_2 of the crystal, these values are only slightly raised by anharmonicity to a 20.7% and a 16.6%, respectively. The reason of this rather small change is a big part of the high energy modes are enhanced by anharmonicity, compensating the softening of the transverse acoustic branches.

As most of the phases have been found and characterized by Raman and infrared spectroscopy experiments, we show the impact of anharmonicity in the optical modes at the Γ point in Table I. The structure has two Raman active modes that are barely affected by anharmonicity.

C. Superconductivity

In order to analyze how anharmonicity affects superconductivity, we have calculated Eliashberg's function $\alpha^2 F(\omega)$ at 500 GPa both in the harmonic and anharmonic cases as described in Sec. II. The $\alpha^2 F(\omega)$ shows a large peak at high energy due to the large electron-phonon linewidth of high-energy optical modes (see Fig. 6). The practically linear and homogeneous increase of

the integrated electron-phonon coupling constant $\lambda(\omega) = 2 \int_0^\omega d\omega' \alpha^2 F(\omega')/\omega'$ indicates that the contribution to the electron-phonon coupling constant is quite homogeneous over all the modes in the BZ. This is true both in the harmonic and in the anharmonic case. Even if anharmonic effects have a significant impact on the phonon spectra, the electron-phonon coupling constant $\lambda = \lambda(\infty)$, which scales with the phonon frequencies as $\propto \omega^{-2}$, is practically unaltered by anharmonicity, as we obtain $\lambda = 1.68$ and $\lambda = 1.63$ in the harmonic and anharmonic cases, respectively. The contribution of the low-energy transverse acoustic modes to the electron-phonon coupling constant is slightly enhanced due to the anharmonic suppression of their frequencies. This is compensated by the hardening of the high-energy optical modes that suppresses λ . The result is that anharmonicity slightly affects the electron-phonon coupling constant.

We estimate the superconducting critical temperature by solving isotropic Migdal-Eliashberg equations in order to overcome the underestimation of T_c given by McMillan's equation in the strongly interacting limit⁴⁴. With a Coulomb pseudopotential of $\mu^* = 0.1$ we obtain a superconducting energy gap (first Matsubara frequency) of $\Delta \approx 62$ meV and $\Delta \approx 58$ meV, respectively, in the harmonic and anharmonic cases at 0 K (see Fig. 7). T_c , defined as the temperature at which the gap vanishes, is 318 K and 300 K respectively in the harmonic and anharmonic approaches. The harmonic result is in reasonable agreement with previous results⁸. The effect of the Coulomb pseudopotential in T_c is weak as it happens in strongly interacting electron-phonon superconductors. Therefore, anharmonicity slightly lowers the superconducting critical temperature in tetragonal $I4_1/amd$ hydrogen due to the small reduction of λ . In Fig. 7 we also show the first Matsubara frequencies of the energy gap at 400 GPa and 600 GPa in the harmonic approach. As we can see, T_c is very weakly affected by pressure in the 400-600 GPa pressure range. Due to the flatness of T_c and the smooth change of the phonons with pressure (Fig. 3) anharmonic effects are expected to have a similar impact at the 400 and 600 GPa.

Considering that in all superconducting hydrides where strong anharmonic effects in superconductivity have been reported there are strongly softened optical modes in the harmonic approximation^{32,34-37}, even imaginary sometimes, it seems the impact of anharmonicity on T_c is largely determined by the presence of such soft hydrogen-character optical modes. Due to the fairly uniform distribution of the electron-phonon coupling in the BZ here, there are no particular optical modes that soften, making anharmonic effects on T_c weaker.

IV. CONCLUSIONS

In this work we have presented an exhaustive analysis of the electronic and vibrational properties of $I4_1/amd$ hydrogen within the 400-600 GPa pressure range. Atomic

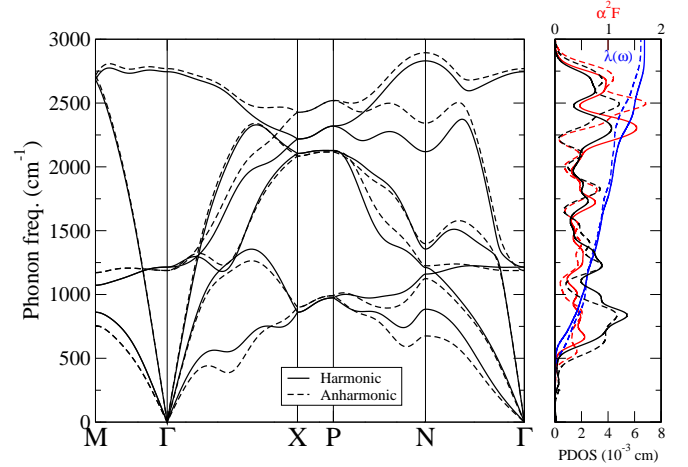


Figure 6. Left: harmonic and anharmonic phonon spectra of $I4_1/amd$ hydrogen at 500 GPa. Right: harmonic and anharmonic phonon density of states (PDOS), electron-phonon Eliashberg's function $\alpha^2 F(\omega)$ and frequency dependent electron-phonon coupling constant $\lambda(\omega)$.

metallic hydrogen in this phase shows a nearly free-electron-like electronic band structure, where the opened band gaps can be explained even without the need of electron-electron interaction. The huge kinetic energy of the electrons due to the extremely high pressure plus their strong interaction with the bare nuclei makes the electron-electron interaction be irrelevant for the electronic structure. Nevertheless, the strong electron-proton interaction creates a big electronic localization near the atomic nuclei. Consequently, the RPA dramatically fails when calculating the phonons of atomic hydrogen. In fact, the inclusion of exchange-correlation effects in the calculation of the electronic response to proton motion guarantees the dynamical stability of the structure.

Despite anharmonicity modifies phonon frequencies up to approximately a 20%, for instance, lowering the energies of the transverse acoustic modes and hardening high-energy optical modes, it has a minor effect on superconductivity, only suppressing T_c by a 6%. This is in stark contrast to other hydrides where anharmonicity has a huge impact on the superconducting properties^{32,34-37}, even inducing an inverse isotope effect in palladium hydrides³⁴. This raises the interesting question whether anharmonicity impacts superconductivity in hydrides simply because hydrogen is light and vibrates far from equilibrium or for another particular reason. Our results suggest that determining whether anharmonicity has a strong impact on T_c cannot be related exclusively to the lightness of the ions present in the system, but to the presence of softened optical modes.

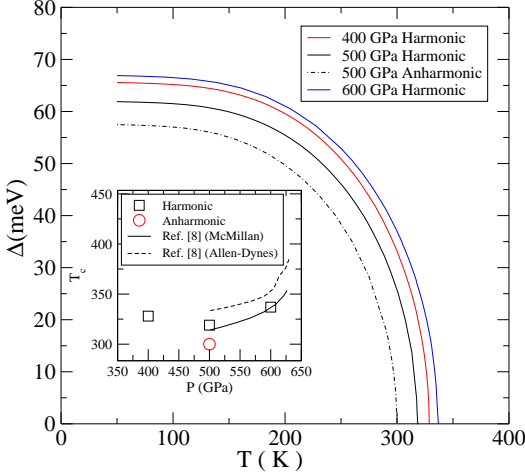


Figure 7. Calculated first Matsubara frequency of the superconducting energy gap of $I4_1/AMD$ hydrogen at different pressures and temperatures using a Coulomb pseudopotential $\mu^* = 0.10$. Inset: T_c vs pressure in the harmonic and anharmonic cases. Solid and dashed curves correspond to the values estimated in Ref. 8, with $\mu^* = 0.089$.

APPENDIX

Within DFT the electronic wave-functions $|\psi_i\rangle$ are calculated diagonalizing the

$$H = T_e + V_{scf} \quad (1)$$

Hamiltonian as $H |\psi_i\rangle = \varepsilon_i |\psi_i\rangle$, where ε_i is the electronic eigenvalue, T_e is the electronic kinetic energy, and the self-consistent potential is

$$V_{scf} = V_{e,p} + V_H + V_{xc}. \quad (2)$$

$V_{e,p}$, V_H , and V_{xc} are, respectively, the electron-proton, Hartree, and exchange-correlation potentials. The different band structures shown in Fig. 2a are obtained neglecting different terms in Eq. (1). The DFT result, of course, retains all the terms in V_{scf} ; in the free-electron approximation $V_{scf} = 0$; and in the independent electron approximation $V_{scf} = V_{e,p}$. We call the latter approach independent electron because in this case electrons do not interact with each other via the V_H and V_{xc} potentials, which depend on the electronic density n .

The electronic part of the dynamical matrix D_e is obtained Fourier transforming the electronic contribution to the force constant matrix, which is given in terms of the electronic density and its derivatives by

$$\begin{aligned} \phi_{i,j}^{\alpha,\beta}(\mathbf{R}) &= \int d\mathbf{r} \left[\frac{\partial n(\mathbf{r})}{\partial u_{i,\mathbf{R}}^\alpha} \right]_0 \left[\frac{\partial V_{e,p}(\mathbf{r})}{\partial u_{j,0}^\beta} \right]_0 \\ &+ \int d\mathbf{r} n(\mathbf{r}) \left[\frac{\partial^2 V_{e,p}(\mathbf{r})}{\partial u_{i,\mathbf{R}}^\alpha \partial u_{j,0}^\beta} \right]_0. \end{aligned} \quad (3)$$

Here, \mathbf{R} is a lattice vector and $u_{i,\mathbf{R}}^\alpha$ is the displacement in the Cartesian direction α of atom i in the unit cell

belonging to the cell defined by \mathbf{R} . The calculation of D_e requires thus the knowledge of the δn the linear change of the electronic density with respect to the ionic displacements. Making use of the electronic density-response function $\chi(\mathbf{r}, \mathbf{r}')$ the linear change of the density can be calculated as

$$\delta n(\mathbf{r}) = \int d\mathbf{r}' \chi(\mathbf{r}, \mathbf{r}') \delta V_{e,p}(\mathbf{r}'), \quad (4)$$

where $\delta V_{e,p}(\mathbf{r})$ represents the linear change of the electron-proton potential. The density response function is usually calculated by first estimating the noninteracting response function $\chi_0(\mathbf{r}, \mathbf{r}')$, which can be directly calculated from the eigenvalues and eigenfunctions of the Hamiltonian in Eq. (1) as

$$\chi^0(\mathbf{r}, \mathbf{r}') = \sum_{i,j} \frac{f_i - f_j}{\varepsilon_i - \varepsilon_j} \psi_i^*(\mathbf{r}) \psi_j(\mathbf{r}) \psi_j^*(\mathbf{r}') \psi_i(\mathbf{r}'), \quad (5)$$

where f_i represents the Fermi-Dirac occupation of the i -th state. The reason for it is that the linear change of density can be given as

$$\delta n(\mathbf{r}) = \int d\mathbf{r}' \chi^0(\mathbf{r}, \mathbf{r}') \delta V_{scf}(\mathbf{r}'). \quad (6)$$

in terms of the noninteracting response function and the linear change of the self-consistent potential. Combining Eqs. (4) and (6), with the linear change of the potential the following self-consistent Dyson-like equation can be obtained for the response function:

$$\begin{aligned} \chi(\mathbf{r}, \mathbf{r}') &= \chi_0(\mathbf{r}, \mathbf{r}') \\ &+ \int d\mathbf{r}_1 d\mathbf{r}_2 \chi_0(\mathbf{r}, \mathbf{r}_1) K(\mathbf{r}_1, \mathbf{r}_2) \chi(\mathbf{r}_2, \mathbf{r}'), \end{aligned} \quad (7)$$

with

$$K(\mathbf{r}, \mathbf{r}') = \frac{1}{|\mathbf{r} - \mathbf{r}'|} + \frac{\partial^2 E_{xc}}{\partial n(\mathbf{r}) \partial n(\mathbf{r}')} \quad (8)$$

and E_{xc} the exchange-correlation energy. If $\delta V_{xc}(\mathbf{r})$ is neglected in Eq. (6), $K(\mathbf{r}, \mathbf{r}') = \frac{1}{|\mathbf{r} - \mathbf{r}'|}$. This is the RPA approximation. Neglecting different contributions for V_{scf} in Eq. (2) one can understand which are the important contributions to the non-interacting $\chi_0(\mathbf{r}, \mathbf{r}')$. Similarly, neglecting different terms in δV_{scf} in Eq. (6) the important contributions to $\chi(\mathbf{r}, \mathbf{r}')$ can be determined.

DFPT³⁸ offers a much more efficient method to calculate δn avoiding the cumbersome calculation of the response function, which requires a slowly converging sum over excited states as shown in Eq. (5). Within DFPT the Sternheimer equation

$$(T_e + V_{scf} - \varepsilon_i) |\delta \psi_i\rangle = -(\delta V_{scf} - \delta \varepsilon_i) |\psi_i\rangle, \quad (9)$$

is solved self-consistently. Here, $\delta \varepsilon_i$ and $|\delta \psi_i\rangle$ are, respectively, the linear change of the electronic eigenvalues and eigenfunctions. Once the Sternheimer equation is

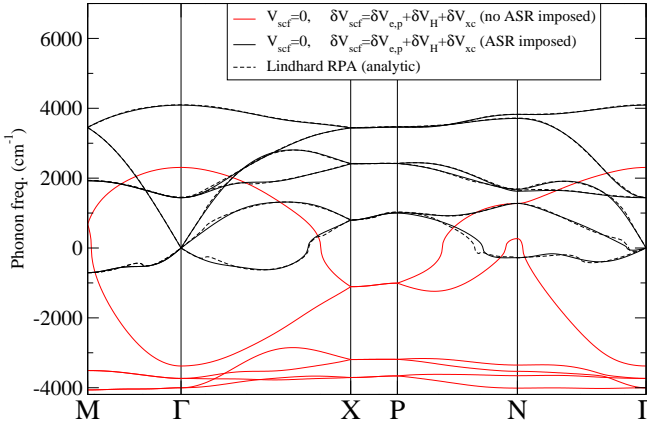


Figure 8. Phonon spectra of $I4_1/AMD$ hydrogen at 500 GPa calculated within DFPT using $V_{scf} = 0$ and $\delta V_{scf} = \delta V_{e,p} + \delta V_H$ with and without imposing the ASR. The results are compared to the Lindhard RPA spectrum calculated analytically, which is an equivalent calculation.

solved and the $|\delta\psi_i\rangle$ states are known, δn can be calculated and, consequently, D_e ³⁸. By neglecting in Eq. (9) different terms in V_{scf} and δV_{scf} we are able to make different implicit approaches to χ_0 and χ , respectively, as described in the previous paragraph.

It is important to note that every time the approaches for V_{scf} and δV_{scf} are different (i.e. the neglected terms are not the same) translational invariance is broken down. The reason is that the ground state densities given by the different approximations differ. In those cases, we impose the ASR *a posteriori* by correcting the force-constants matrix in Eq. (3) as

$$\tilde{\phi}_{i,i}^{\alpha,\beta}(0) = \phi_{i,i}^{\alpha,\beta}(0) - \sum_{\mathbf{R},j} \phi_{i,j}^{\alpha,\beta}(\mathbf{R}) \quad (10)$$

for every possible i , α and β . The new $\tilde{\phi}$ yield dynamical matrices that satisfy the ASR. This way of imposing the ASR is equivalent to correcting the second addend in Eq. (3) *a posteriori*, which gives a non-dispersive term to the dynamical matrix as the correction in Eq. (10). As an example, in Fig. 8 we show how imposing of the ASR works in the case $V_{scf} = 0$, $\delta V_{scf} = \delta V_{e,p} + \delta V_H$, which is equivalent to the analytic Lindhard RPA approximation. We see how after imposing the ASR the spectrum coincides with the analytic one. The small differences between the analytic spectrum and the one obtained with the DFPT procedure are because the latter is obtained from a Fourier interpolation from a $6 \times 6 \times 6$ \mathbf{q} -grid, while

the former is calculated point by point.

The phonon-spectra presented in Fig. 5 are calculated solving Eq. (9) in three different ways: i) taking $V_{scf} = V_{e,p}$ and $\delta V_{scf} = \delta V_{e,p} + \delta V_H + \delta V_{xc}$; ii) taking $V_{scf} = V_{e,p}$ but neglecting the linear change of the

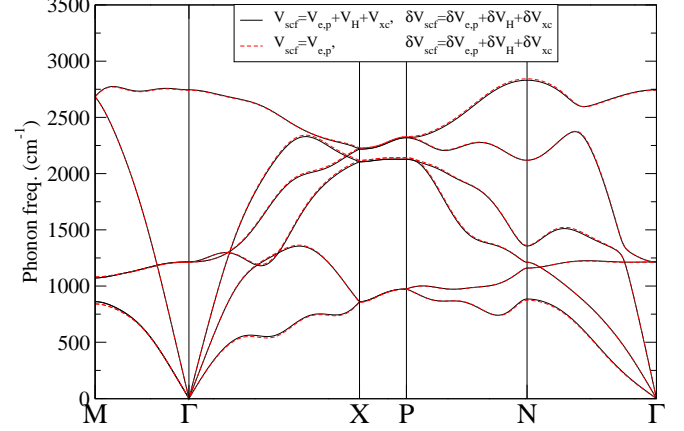


Figure 9. Phonon spectra of $I4_1/AMD$ hydrogen at 500 GPa calculated within DFPT using two different approaches for V_{scf} . In the $V_{scf} = V_{e,p}$ and $\delta V_{scf} = \delta V_{e,p} + \delta V_H + \delta V_{xc}$ calculation the ASR is imposed *a posteriori*.

it ($\delta V_{scf} = \delta V_{e,p} + \delta V_H + \delta V_{xc}$). In Fig. 9 we show how the inclusion of the electron-electron interaction in V_{scf} is irrelevant, as one obtains the same spectra as including it (after imposing ASR in the first case).

ACKNOWLEDGEMENTS

The authors acknowledge financial support from the Spanish Ministry of Economy and Competitiveness (FIS2013-48286-C2-2-P), the Department of Education, Universities and Research of the Basque Government and the University of the Basque Country (IT756-13), and French Agence Nationale de la Recherche (Grant No. ANR-13-IS10-0003-01). M.B. is also thankful to the Department of Education, Language Policy and Culture of the Basque Government for a predoctoral fellowship (Grant No. PRE-2014-1-477). Computer facilities were provided by the Donostia International Physics Center (DIPC).

¹ A. P. Drozdov, M. I. Eremets, I. A. Troyan, V. Ksenofontov, and S. I. Shylin, *Nature* **525**, 73 (2015).

² N. W. Ashcroft, *Phys. Rev. Lett.* **21**, 1748 (1968).

³ N. W. Ashcroft, *Phys. Rev. Lett.* **92**, 187002 (2004).

⁴ P. Cudazzo, G. Profeta, A. Sanna, A. Floris, A. Continenza, S. Massidda, and E. K. U. Gross, *Phys. Rev. Lett.* **100**, 257001 (2008).

⁵ L. Zhang, Y. Niu, Q. Li, T. Cui, Y. Wang, Y. Ma, Z. He, and G. Zou, *Solid State Communications* **141**, 610 (2007).

- ⁶ P. Cudazzo, G. Profeta, A. Sanna, A. Floris, A. Continenza, S. Massidda, and E. K. U. Gross, *Phys. Rev. B* **81**, 134505 (2010).
- ⁷ P. Cudazzo, G. Profeta, A. Sanna, A. Floris, A. Continenza, S. Massidda, and E. K. U. Gross, *Phys. Rev. B* **81**, 134506 (2010).
- ⁸ J. M. McMahon and D. M. Ceperley, *Phys. Rev. B* **84**, 144515 (2011).
- ⁹ Y. Yan, J. Gong, and Y. Liu, *Physics Letters A* **375**, 1264 (2011).
- ¹⁰ E. Maksimov and D. Savrasov, *Solid State Communications* **119**, 569 (2001).
- ¹¹ M. I. Eremets, I. A. Troyan, and A. P. Drozdov, *arXiv:1601.04479*.
- ¹² P. Loubeyre, R. LeToullec, D. Hausermann, M. Hanfland, R. J. Hemley, H. K. Mao, and L. W. Finger, *Nature* **383**, 702 (1996).
- ¹³ S. Deemyad and I. F. Silvera, *Phys. Rev. Lett.* **100**, 155701 (2008).
- ¹⁴ A. B. Stanimir, E. Schwegler, T. Ogitsu, and G. Galli, *Nature* **431**, 669 (2004).
- ¹⁵ H.-k. Mao and R. J. Hemley, *Rev. Mod. Phys.* **66**, 671 (1994).
- ¹⁶ C.-S. Zha, Z. Liu, and R. J. Hemley, *Phys. Rev. Lett.* **108**, 146402 (2012).
- ¹⁷ A. F. Goncharov, E. Gregoryanz, R. J. Hemley, and H.-k. Mao, *Proceedings of the National Academy of Sciences* **98**, 14234 (2001).
- ¹⁸ M. I. Eremets and I. A. Troyan, *Nat Mater* **10**, 927 (2011).
- ¹⁹ R. T. Howie, C. L. Guillaume, T. Scheler, A. F. Goncharov, and E. Gregoryanz, *Phys. Rev. Lett.* **108**, 125501 (2012).
- ²⁰ C.-s. Zha, Z. Liu, M. Ahart, R. Boehler, and R. J. Hemley, *Phys. Rev. Lett.* **110**, 217402 (2013).
- ²¹ R. T. Howie, P. Dalladay-Simpson, and E. Gregoryanz, *Nat Mater* **14**, 495 (2015).
- ²² P. Dalladay-Simpson, R. T. Howie, and E. Gregoryanz, *Nature* **529**, 63 (2016).
- ²³ P. Loubeyre, F. Occelli, and R. LeToullec, *Nature* **416**, 613 (2002).
- ²⁴ C. J. Pickard and R. J. Needs, *Nat Phys* **3**, 473 (2007).
- ²⁵ C. J. Pickard, M. Martinez-Canales, and R. J. Needs, *Phys. Rev. B* **85**, 214114 (2012).
- ²⁶ L. Dubrovinsky, N. Dubrovinskaia, E. Bykova, M. Bykov, V. Prakapenka, C. Prescher, K. Glazyrin, H.-P. Liermann, M. Hanfland, M. Ekholm, Q. Feng, L. V. Pourovskii, M. I. Katsnelson, J. M. Wills, and I. A. Abrikosov, *Nature* **525**, 226 (2015).
- ²⁷ S. Azadi, B. Monserrat, W. M. C. Foulkes, and R. J. Needs, *Phys. Rev. Lett.* **112**, 165501 (2014).
- ²⁸ J. M. McMahon and D. M. Ceperley, *Phys. Rev. Lett.* **106**, 165302 (2011).
- ²⁹ N. D. Drummond, B. Monserrat, J. H. Lloyd-Williams, P. L. Rios, C. J. Pickard, and R. J. Needs, *Nat Commun* **6** (2015), article.
- ³⁰ I. B. Magdau and G. J. Ackland, *Phys. Rev. B* **87**, 174110 (2013).
- ³¹ H. Liu and Y. Ma, *Phys. Rev. Lett.* **110**, 025903 (2013).
- ³² I. Errea, M. Calandra, C. J. Pickard, J. Nelson, R. J. Needs, Y. Li, H. Liu, Y. Zhang, Y. Ma, and F. Mauri, *Phys. Rev. Lett.* **114**, 157004 (2015).
- ³³ I. Errea, M. Calandra, C. J. Pickard, J. R. Nelson, R. J. Needs, Y. Li, H. Liu, Y. Zhang, Y. Ma, and F. Mauri, *Nature* **532**, 81 (2016).
- ³⁴ I. Errea, M. Calandra, and F. Mauri, *Phys. Rev. Lett.* **111**, 177002 (2013).
- ³⁵ I. Errea, M. Calandra, and F. Mauri, *Phys. Rev. B* **89**, 064302 (2014).
- ³⁶ B. Rousseau and A. Bergara, *High Pressure Research* **31**, 30 (2011).
- ³⁷ B. Rousseau and A. Bergara, *Phys. Rev. B* **82**, 104504 (2010).
- ³⁸ S. Baroni, S. de Gironcoli, A. Dal Corso, and P. Giannozzi, *Rev. Mod. Phys.* **73**, 515 (2001).
- ³⁹ J. P. Perdew, K. Burke, and M. Ernzerhof, *Phys. Rev. Lett.* **77**, 3865 (1996).
- ⁴⁰ P. Giannozzi *et al.*, *J. Phys. Condens. Matter* **21**, 395502 (2001) (2009).
- ⁴¹ B. Rousseau, I. Errea, and A. Bergara, *Journal of Physics and Chemistry of Solids* **71**, 1159 (2010).
- ⁴² A. B. Migdal, Sov. Phys. JETP **7**, 996 (1958).
- ⁴³ G. M. Eliashberg, Sov. Phys. JETP **11**, 696 (1960).
- ⁴⁴ P. B. Allen and R. C. Dynes, *Phys. Rev. B* **12**, 905 (1975).
- ⁴⁵ K. Nagao, S. A. Bonev, A. Bergara, and N. W. Ashcroft, *Phys. Rev. Lett.* **90**, 035501 (2003).
- ⁴⁶ B. Rousseau, Y. Xie, Y. Ma, and A. Bergara, *Eur. Phys. J. B* **81**, 1 (2011).
- ⁴⁷ C. Lee, W. Yang, and R. G. Parr, *Phys. Rev. B* **37**, 785 (1988).
- ⁴⁸ C. Bowen, G. Sugiyama, and B. J. Alder, *Phys. Rev. B* **50**, 14838 (1994).
- ⁴⁹ S. Azadi and W. M. C. Foulkes, *Phys. Rev. B* **88**, 014115 (2013).
- ⁵⁰ C. A. Burns and E. D. Isaacs, *Phys. Rev. B* **55**, 5767 (1997).